RAPID COMMUNICATIONS

PHYSICAL REVIEW B VOLUME 50, NUMBER 23 15 DECEMBER 1994-I

Plasmons and optical properties of carbon nanotubes

M. F. Lin and Kenneth W.-K. Shung
Physics Department, National Tsing Hua University, Hsinchu, Taiwan 30043, The Republic of China
(Received 30 September 1994)

The optical properties of carbon nanotubes are studied within the gradient approximation. The calculated dielectric function exhibits many divergent structures, due to the divergencies in its density of states. As a result, the electron-energy-loss spectrum has many peak structures, including a prominent one at ~6 eV, which is identified as the collective excitations of the π-band electrons. This plasmon is found to be insensitive to both radius and chiral angle, due to the unique one-dimensional band structure of carbon nanotubes. The result is consistent with the experimental measurements. The reflectance also exhibits many interesting features, including a weak but sharp plasmon edge at ~6 eV.

Iijima[1] recently reported observation of carbon nanotubes, which are graphite sheets rolled up in the cylindrical form. These nanotubes, with radii between 10 and 150 Å, represent an interesting class of one-dimensional (1D) systems. This system has generated many interesting studies on its structural,[2–4] electronic,[5–11] magnetic,[12,13] and transport properties.[14] The objective of this paper is to investigate the basic optical properties of the carbon nanotubes by means of evaluating their dielectric function $\epsilon(\omega)$.

The system under consideration consists of a bundle of identical, single-shell nanotubes that have their axes parallel to each other. The dielectric function is evaluated within the gradient approximation,[15] which has been applied, with success, to graphite[15] and graphite intercalation compounds (GIC's).[16] We assume that the polarization of the electromagnetic (em) field is parallel to the tubular axis. Other polarization angles will be discussed elsewhere.[17] In the evaluation of $\epsilon(\omega)$, the intertube interaction is neglected, but the band structure is taken into account within the tight-binding method. Correct description of the band is found to be very important in this study.

A carbon nanotube has subbands that, in general, exhibit typical 1D character with a divergent density of states (DOS) at the band edge. As a result, there are many divergent structures in $\epsilon(\omega)$ and peak structures in reflectance $[R(\omega)]$. Also present in $R(\omega)$ is a Drude-like, but weaker edge at $\omega\sim 6$ eV ($\hbar=1$), which is identified as a collective mode due to the π electrons. This plasmon mode has been studied in detail and its unique characters are found to originate from the special band structure of the graphitelike system. Our study shows that the plasmon structure is insensitive to changes in both the radius and the chiral angle of the nanotube, and always lies at 6–7 eV. This result may well explain the ~5–7-eV plasmon found in the electron-energy-loss spectrum (EELS) of multishell carbon nanotubes.[8–11]

A carbon nanotube, as shown in Fig. 1(a), is a rolled up graphite sheet such that the carbon atom at origin coincides with another carbon at $\mathbf{R}=m\mathbf{a}_1+n\mathbf{a}_2$, where $\mathbf{a}_1=\sqrt{3}b\mathbf{e}_x$ and $\mathbf{a}_2=(\sqrt{3}/2)b\mathbf{e}_x-\frac{3}{2}b\mathbf{e}_y$ are the primitive lattice vectors of the graphite sheet, and $\mathbf{e}_x$ ($\mathbf{e}_y$) is the unit vector along the x axis (y axis). The nearest-neighbor distance $b=1.42$ Å. The geometry of a nanotube is completely determined once $\mathbf{R}$ is determined. One can thus specify a nanotube by the parameters (m,n). For example, the zigzag tubule that has $\mathbf{R}\|\mathbf{e}_x$ is denoted by $(m,0)$. The (23,0) tubule, which has a small radius $r=9$ Å, is chosen here for a detailed study. It reveals that the unique 1D band structure causes the prominent ~6-eV plasmon structure in all nanotubes. Some results[17] calculated from other tubules will be presented here to illustrate this common feature.

The electronic structure of a zigzag is calculated within the tight-binding model, which is similar to the one employed for a graphite sheet.[18] The π-band structure of a graphite sheet is caused by the overlapping carbon $2p_z$ orbitals, which belong to two sublattices. The Hamiltonian in the subspace spanned by the two tight-binding functions $U_1(k_x,k_y)$ and $U_2(k_x,k_y)$ is thus described by a 2×2 matrix,[18]

$$H=\begin{pmatrix} 0 & H_{12}(k_x,k_y) \\ H_{12}^*(k_x,k_y) & 0 \end{pmatrix}, \tag{1}$$

where $H_{12}(k_x,k_y)=-\gamma_0\Sigma_{i=1}^{3}e^{-i\mathbf{k}\cdot\mathbf{r}_i}$. The Hamiltonian only contains the interactions of each carbon atom with its three nearest neighbors, denoted by $\mathbf{r}_i$. The quantity $\gamma_0=3.033$ eV (Ref. 7) is the resonance integral, and $\mathbf{k}$ is the Bloch wave vector. The Bloch states of Eq. (1) when applied to the nanotubes, must satisfy the boundary condition

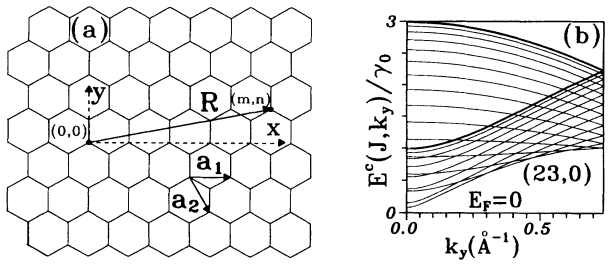

FIG. 1. (a) The vector $\mathbf{R}$ defines a carbon nanotube in terms of a graphite sheet. (b) The conduction bands of the (23,0) tubule. The occupied valence bands are symmetric, about $E_F=0$, to the conduction bands.

$$\Psi(\mathbf{r})=\Psi(\mathbf{r}+\mathbf{R}), \tag{2}$$

where $\mathbf{R}$ is the vector that defines the tubule. For a zigzag nanotube, the boundary condition requires that the transverse wave vector $k_x=2\pi J/\sqrt{3}mb$ ($J=1,2,\ldots,2m$); the J's thus serve as good quantum numbers for the subbands. The axial wave vector is confined to the first Brillouin zone $|k_y|\leq\pi/3b$, and $k_y=0$ corresponds to the band edge. The π-band energy dispersions of the $(m,0)$ tubule are obtained from diagonalizing the Hamiltonian:

$$E^{c,v}(J,k_y)=\pm\gamma_0\left\{1+4\cos\left(\frac{3bk_y}{2}\right)\cos\left(\frac{J\pi}{m}\right)+4\cos^2\left(\frac{J\pi}{m}\right)\right\}^{1/2}, \tag{3a}$$

and the wave functions are

$$\Psi^{c,v}(J,k_y)=\frac{1}{\sqrt{2}}\left\{U_1(J,k_y)\mp\frac{H_{12}^*(J,k_y)}{|H_{12}(J,k_y)|}U_2(J,k_y)\right\}. \tag{3b}$$

The superscript c (v) represents the conduction (valence) band. The nanotubes with $2m+n=3\times$integer are metallic; otherwise, they are semiconducting.[5–7] The (23,0) tubule is thus a semiconductor with a 0.48-eV band gap; its band structure is given in Fig. 1(b). All the subbands are doubly degenerate except the two with $J=m$ and $2m$.

The (23,0)-nanotube bundle[3,4] is assumed to have a density of one tubule per $(2r+d)^2$ Å^2, which corresponds to that of a square-lattice structure. $d=3.4$ Å is the intertube distance.[1] Only the density is relevant here since the intertube interaction among the nanotubes has been neglected. Then $\epsilon(\omega)$ is essentially determined by a single tubule and, within the relaxation-time approximation,[15] it is given by

$$\epsilon(\omega)=\epsilon_0-\frac{8\pi e^2}{\omega(2r+d)^2}\sum_J\int_{1\text{st BZ}}\frac{dk_y}{2\pi}\frac{\left|\left\langle\Psi^c(J,k_y)\left|\frac{P_y}{m_e}\right|\Psi^v(J,k_y)\right\rangle\right|^2}{\omega_{vc}(J,k_y)}\left\{\frac{1}{\omega-\omega_{vc}(J,k_y)+i\Gamma}-\frac{1}{\omega+\omega_{vc}(J,k_y)+i\Gamma}\right\}. \tag{4}$$

Allowed transitions are restricted to the vertical excitations (i.e., J and k_y remain unchanged) from the valence bands to the conduction bands. This result follows from our assumption that the polarization of the em field is along the axial direction of the nanotubes. Other polarizations have more complicated results.[17] In Eq. (4), $\omega_{vc}(J,k_y)=2E^c(J,k_y)$, i.e., the vertical interband excitation energy. The background dielectric constant $\epsilon_0=2.4$ is taken from graphite.[19] Γ is the energy width due to various deexcitation mechanisms, and is treated as a free parameter in the calculation. The velocity matrix element $|\langle\Psi^c(J,k_y)|P_y/m_e|\Psi^v(J,k_y)\rangle|$ may be approximated by taking the gradient of Hamiltonian versus k_y, e.g., $|\langle U_1(J,k_y)|P_y/m_e|U_2(J,k_y)\rangle|\approx\partial H_{12}(J,k_y)/\partial k_y$. The matrix element may then be easily evaluated. Similar approximations have been successfully applied in explaining optical spectra of graphite[15] and GIC's.[16]

The real $[\epsilon_1(\omega)]$ and the imaginary $[\epsilon_2(\omega)]$ parts of the dielectric function of the (23,0) nanotube are shown in Figs. 2(a) and 2(b). The dielectric function becomes essentially featureless above 12 eV and is thus not shown. The profile of $\epsilon(\omega)$ mainly reflects the available channels of optically induced interband excitations. At an energy ω, which corresponds to excitations from states near the band edge, the number of such excitations becomes infinite because of divergent DOS of the 1D subband there. Therefore, there are many divergent structures in $\epsilon(\omega)$. The joint density of states (JDOS) $[D_J(\omega)=\Sigma_J|\partial\omega_{vc}(J,k_y)/\partial k_y|^{-1}_{\omega_{vc}=\omega}]$ is evaluated and shown in Fig. 2(c), which clearly illustrates the correspondence between the 1D DOS and $\epsilon(\omega)$. It should be noted that the JDOS at ω is simply one-half of the DOS of the conduction band at $E^c=\omega/2$. This relation follows from the fact that the conduction bands and the valence bands are symmetric about energy zero [Eq. (3a)]. That $\epsilon(\omega)$ should diminish in magnitude at large ω results from the $1/\omega^2$ factor of Eq. (4). Figures 2(a)–2(c) reveal an important message: the singular structure of the JDOS by and large determines $\epsilon(\omega)$ and, hence, also the optical properties of the 1D nanotubes.

That the conduction bands [Fig. 1(b)] concave upwards at the band edge ($k_y=0$) for $E^c<\gamma_0$ and downwards for $E^c>\gamma_0$ has important consequences as far as the optical properties are concerned. Mainly, the DOS near a band edge at $E^c_{ed}<\gamma_0$ diverges in the form $1/\sqrt{E^c-E^c_{ed}}$ while that at $E^c_{ed}>\gamma_0$ diverges in the form $1/\sqrt{E^c_{ed}-E^c}$. Similar divergences can thus be found at $\omega\sim 2E^c_{ed}$ in the JDOS [Fig. 2(c)], as explained earlier. Corresponding to a concave downward 1D band (i.e., $E^c_{ed}>\gamma_0$), $\epsilon_1(\omega)$ becomes negative and divergent at $\omega\geq 2E^c_{ed}$. This results follows directly from Eq. (4) and can be derived analytically by assuming the dominance of the first term on the right-hand side of the equation.[17] Clearly, $\epsilon_1(\omega)$ must thus have zeros at ω in the neighborhood of $2E^c_{ed}>2\gamma_0$. Zeros in $\epsilon_1(\omega)$, if at where $\epsilon_2(\omega)$ is small, are associated with collective modes, or plasmons, of the system. Plasmons could cause prominent structures in, for example, EELS, which is examined below, as are other optical properties of the nanotubes.

The calculated EELS at zero momentum transfer, which is defined as $\mathrm{Im}[-1/\epsilon(\omega)]$, is shown in Fig. 3 at several different energy widths. The spectral function has many local minima at $\omega<2\gamma_0$, obviously due to the divergent JDOS from the concave-upward subbands. The spectra behave characteristically differently at $\omega>2\gamma_0$. There the divergent JDOS from the concave-downward subbands lead to promi-

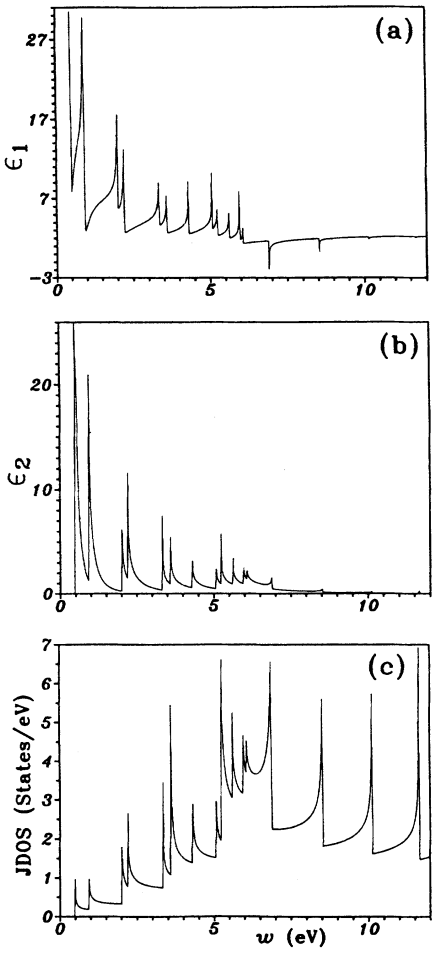

FIG. 2. The calculated results of the (23,0) tubules. (a) $\epsilon_1(\omega)$, (b) $\epsilon_2(\omega)$, and (c) JDOS for the vertical interband transitions.

nent plasmon structures, due to zeros in $\epsilon_1(\omega)$. Several plasmon peaks are found in the spectrum, and each of them is associated with a band edge at $E^c > \gamma_0$. Of these plasmons, the one at the lowest energy $\omega \doteq 2\gamma_0$ is by far the strongest.

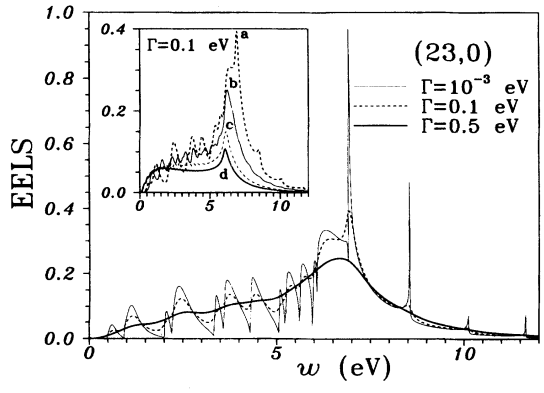

FIG. 3. The calculated EELS at zero momentum transfer for the (23,0) tubules are calculated at various energy widths. The inset shows EELS of four carbon nanotubes: (23,0), (40,10), (72,32), and (78,78), labeled *a*, *b*, *c*, and *d*, respectively ($\Gamma = 0.1$ eV).

The fine details of the EELS become smoothed out at increasing broadening. But even at $\Gamma = 0.5$ eV the plasmon structure at $\sim 2\gamma_0$ remains strong and becomes the only dominating structure in the spectrum. In short, this band-induced 1D plasmon mode at $\sim 2\gamma_0$ is the most important excitation in the loss spectrum.

The properties of the (23,0) nanotube discussed above are found to be generally true to other nanotubes. The inset of Fig. 3 illustrates the EELS ($\Gamma = 0.1$ eV) of different nanotubes, with a wide range of chiral angles and radii. Details of these calculations will be discussed elsewhere.[17] Some of the tubules are metallic and others are semiconducting, but all of them share the common feature—a prominent plasmon structure at $\omega \sim 2\gamma_0$. This result is not accidental but follows from the fact that all carbon nanotubes derive their bands from that of a graphite sheet. Carbon nanotubes of different sizes and chiralities satisfy different boundary conditions, Eq. (2), and their bands are thus all different. But an important common band feature exists, and that is the presence of concave-downward 1D subbands at $E^c \sim \gamma_0$, the origin of the plasmon at $\omega \sim 2\gamma_0$. In terms of the hexagonal Brillouin zone of a graphite sheet,[18] these concave-downward 1D subbands come from the midsection between the degenerate K and K' points. Different carbon nanotubes, following Eq. (2), must all sample this region for allowed states, and thus all have the $\sim 2\gamma_0$ plasmons, as the inset of Fig. 3 shows. Detailed band calculations of the carbon nanotubes may lead to subtle modifications, but they are not expected to change the basic conclusion reached above. It is interesting to note that similar inter-π-band transitions have been suggested to explain an ~ 6-eV plasmon in C_{60}.[20]

The prediction that different carbon nanotubes have approximately the same plasmon energy at $\sim 2\gamma_0 \approx 6$ eV could be experimentally checked, with EELS or other optical measurements. EELS measurements exist[8–11] for multishell carbon nanotubes of different sizes and reveal that a broad, prominent plasmon at ~ 5–7 eV is always observed. This result is consistent with our calculations. Within the independent nanotube approximation, a multishell nanotube can be regarded as a combination of single-shell tubules. The observed plasmon structure is then a superposition of several single-shell plasmons.[17] This picture, crude as it is, may well explain the prominent plasmon structure at ~ 6 eV, and also the shoulders that appear in the measurements.[8]

The calculated EELS of Fig. 3 clearly has several plasmon structures at $\omega > 2\gamma_0$; the weaker ones at higher energies diminish only at fairly large broadening width. These plasmons are caused by a series of concave downward subbands [see Fig. 1(b)]; each of these band edges determines one plasmon frequency. The plasmon strength, given by $\sim |\partial \epsilon_1(\omega)/\partial \omega^2|^{-1}$, may be evaluated from Eq. (4) and is found[17] to be approximately proportional to m^*/ω_p^3 for a plasmon at ω_p; m^* is the effective mass of the subband that determines the plasmon. The plasmon at $\sim 2\gamma_0$, therefore, has the dominating spectral weight while others at higher energies appear as weaker plasmon satellites in the spectra (e.g., at 8.5 and 10 eV of Fig. 3). That some nanotubes may have strong multiple plasmon satellites, however, cannot be ruled out. There exist some evidences of such 1D-subband-

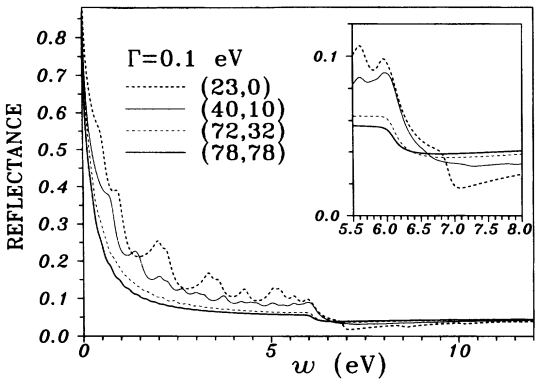

FIG. 4. The calculated reflectance spectra of the nanotubes (23,0), (40,10), (72,32), and (78,78). The inset shows the details at $\omega \sim 6$ eV.

induced plasmon satellites (at ~ 9 eV) in the measurement.[8] Further study is clearly needed to clarify this rather unique feature of carbon nanotubes.

Figure 4 is the reflectance spectra of several nanotubes at $\Gamma = 0.1$ eV, which are calculated from the relation $R(\omega) = |1 - \sqrt{\epsilon(\omega)}|^2 / |1 + \sqrt{\epsilon(\omega)}|^2$. There are many peaks in $R(\omega)$ at $\omega < 2\gamma_0$, clearly due to the divergent JDOS that we discussed earlier. These structures are strong for the (23,0) tubules and gradually diminish as the radii of the nanotubes increase, owing to a rapid increase in the number of subbands. For $\omega > 2\gamma_0$, the reflectance is essentially featureless and can be represented by a Drude tail. At $\omega \sim 2\gamma_0$, where the strong plasmons are located, the clear plasmon edge is observed in $R(\omega)$ (see inset). This edge structure is unique in that it is not as strong as in ordinary metals where the plasmon edge can be described by a one-parameter Drude model, while on the other hand, the plasmon edge of nanotubes is rather sharp (0.1–0.2 eV in width). That it should be so sharp is unexpected since $\epsilon_2(\omega_p)$ is fairly large [Fig. 2(b)], which usually accounts for strong Landau damping of the plasmon mode. It is the rapid and strong fluctuations in the 1D JDOS [Fig. 2(c)] of the nanotubes that cause the unique features in $R(\omega)$.

We have calculated for carbon nanotubes the dielectric function at zero-momentum transfer $\epsilon(\omega)$, which is useful for studying the optical properties. Despite the very complicated band structure, different nanotubes always have a dominating plasmon mode at $2\gamma_0 \sim 6$ eV. The cause and the character of this 6-eV plasmon have been discussed in detail. The findings should have an important bearing on our understanding of this 1D system. Some experimental evidence in support of our results is discussed. Further details, together with a discussion on the magneto-optical properties, will be given elsewhere.[17]

This work was supported in part by the National Science Council of Taiwan, the Republic of China under Grants Nos. NSC 83-0208-M-007-041 and NSC 84-2112-M-007-018.

[1] S. Iijima, Nature **354**, 56 (1991).
[2] S. Iijima and T. Ichihashi, Nature **363**, 603 (1993).
[3] X. K. Wang, X. W. Lin, V. P. Dravid, J. B. Ketterson, and R. P. H. Chang, Appl. Phys. Lett. **62**, 1881 (1993).
[4] M. Ge and K. Sattler, Appl. Phys. Lett. **64**, 710 (1994).
[5] J. W. Mintwire, B. I. Dunlap, and C. T. White, Phys. Rev. Lett. **68**, 631 (1992).
[6] N. Hamada, S. I. Sawada, and A. Oshiyama, Phys. Rev. Lett. **68**, 1579 (1992).
[7] R. Saito, F. Fujita, G. Dresselhaus, and M. S. Dresselhaus, Appl. Phys. Lett. **60**, 2204 (1992); Phys. Rev. B **46**, 1804 (1992).
[8] R. Kuzuo, M. Terauchi, and M. Tanaka, J. Phys. Soc. Jpn. **31**, L1484 (1992).
[9] P. M. Ajayan, S. Iijima, and T. Ichihashi, Phys. Rev. B **47**, 6859 (1993).
[10] V. P. Dravid, X. W. Lin, Y. Wang, X. K. Wang, A. Yee, J. B. Ketterson, and R. P. H. Chang, Science **259**, 1601 (1993).
[11] L. A. Bursill, P. A. Stadelmann, J. L. Peng, and S. Prawer, Phys. Rev. B **49**, 2882 (1994).
[12] H. Ajiki and T. Ando, J. Phys. Soc. Jpn. **62**, 2470 (1993).
[13] M. F. Lin and K. W.-K. Shung, Phys. Rev. B **48**, 5567 (1993).
[14] W. Tian and S. Datta, Phys. Rev. B **49**, 5097 (1994).
[15] L. G. Johnson and G. Dresselhaus, Phys. Rev. B **7**, 2275 (1973).
[16] J. Blinowski, N. H. Hau, C. Rigaux, J. P. Vieren, R. L. Toullee, G. Furdin, A. Herold, and J. Melin, J. Phys. (Paris) **41**, 47 (1980).
[17] M. F. Lin and K. W.-K. Shung (unpublished).
[18] P. R. Wallace, Phys. Rev. **71**, 622 (1947).
[19] E. A. Taft and H. R. Philipp, Phys. Rev. **138**, A197 (1965).
[20] G. Gensterblum, J. J. Pireaux, P. A. Thiry, R. Caudano, J. P. Vigneron, Ph. Lambin, and A. A. Lucas, Phys. Rev. Lett. **67**, 2171 (1991).